

Structure and mechanical properties of B2 ordered refractory AlNbTiVZr_x (x = 0–1.5) high-entropy alloys



N.Yu. Yurchenko^{a,*}, N.D. Stepanov^a, S.V. Zharebtsov^a, M.A. Tikhonovsky^b, G.A. Salishchev^a

^a Laboratory of Bulk Nanostructured Materials, Belgorod State University, Belgorod 308015, Russia

^b National Science Center “Kharkov Institute of Physics and Technology” NAS of Ukraine, Kharkov 61108, Ukraine

ARTICLE INFO

Keywords:

A. Electron Microscopy
X-ray analysis
B. High-entropy alloys
D. Phase transformation
B2 structure
Disordering

ABSTRACT

Structure and mechanical properties of the AlNbTiVZr_x (x = 0; 0.1; 0.25; 0.5; 1; 1.5) refractory high-entropy alloys were investigated after arc melting and annealing at 1200 °C for 24 h. The AlNbTiV alloy had a B2 ordered single phase structure. Alloying with Zr resulted in (i) change of the degree of order of the B2 phase; and (ii) precipitation of the Zr₅Al₃ and C14 Laves ZrAlV phases. The density of the AlNbTiVZr_x alloys varied from 5590 kg m⁻³ for the AlNbTiV alloy to 5870 kg m⁻³ for the AlNbTiVZr_{1.5} alloy. The compression yield strength at 22 °C increased with an increase in the Zr content from 1000 MPa for the AlNbTiV alloy to 1535 MPa for the AlNbTiVZr_{1.5} alloy. The plasticity raised from 6% for the AlNbTiV alloy to > 50% for the AlNbTiVZr_{0.5} alloy and then dropped to 0.4% for the AlNbTiVZr_{1.5} alloy. At 600 °C, the strongest alloy was also the AlNbTiVZr_{1.5}, whereas, at 800 °C, the AlNbTiVZr_{0.1} alloy demonstrated the maximum strength. The plasticity of the AlNbTiV alloy at 600 °C increased up to 14.3%, while the Zr-containing alloys had lower plasticity. At 800 °C, all the AlNbTiVZr_x alloys could be plastically deformed up to 50% of strain without fracture. Ordering in the alloys and the reasons of a complicated dependence of mechanical properties of the AlNbTiVZr_x alloys on the Zr content and temperature were discussed.

1. Introduction

So-called high-entropy alloys (HEAs) provide a new tempting approach to creation and elaboration of materials with outstanding properties [1–3]. According to the original definition [1], HEAs composed of 5 or more principal elements taken into equiatomic or nearly equiatomic proportions. However, alloys with four constitutive elements can also be considered as HEAs. [4–9]. Conversion from a single-basic-element approach to the multi-component one allows the development of new alloys with highly promising properties for various potential applications [5,7,10,11]. For example, refractory HEAs introduced by Senkov et al. in 2010 demonstrated very high strength up to 1600 °C [5]. However, the density of these HEAs (> 10 g/cm³) is noticeably higher than that of commercial superalloys. The necessity to decrease the density of these alloys served as a trigger for the developing new light-weight refractory HEAs [6–8,12–16].

Obvious approaches to develop refractory HEAs with low weight are: (i) using elements with high melting points and relatively low density (like Cr, Nb, Ti, V, Zr) and (ii) adding light-weight metals such as Al. Stepanov et al. [8] introduced an equiatomic single phase AlNbTiV alloy with the density of 5.59 g/cm³. This alloy exhibited

surprisingly high specific strength up to 800 °C but poor plasticity at room temperature. Aluminum was thought to be responsible for the properties demonstrated by the AlNbTiV alloy [8]. Addition of Cr to the AlNbTiV alloy has resulted in the formation of Laves phase particles and further increase in the strength at room and elevated temperatures [13]. However, room temperature ductility of the AlCr_xNbTiV alloys decreased pronouncedly with an increase in the Cr content. In contrast, alloying the AlNbTiV alloy with 0.5 M fraction of Zr provided a drastic increase in the room-temperature plasticity [14]. This is an interesting finding since the alloy possesses good plasticity despite a relatively high amount (~15 vol%) of intermetallic phases. The reasons for a considerable growth in plasticity of the AlNbTiV alloy at ambient temperature in the presence of Zr were not clarified so far. In the current study an effort to elucidate this issue was made. For that purpose, structure of the AlNbTiVZr_x alloys with different Zr content was analyzed and the effect of Zr on mechanical properties of the AlNbTiV alloy was evaluated.

2. Experimental procedures

The alloys with a nominal composition of AlNbTiV, AlNbTiVZr_{0.1},

* Corresponding author.

E-mail address: yurchenko_nikita@bsu.edu.ru (N.Y. Yurchenko).

AlNbTiVZr_{0.25}, AlNbTiVZr_{0.5}, AlNbTiVZr, and AlNbTiVZr_{1.5} were produced by arc melting of the elements in a low-pressure, high-purity argon atmosphere inside a water-cooled copper cavity. The purities of the alloying elements were no less than 99.9 at%. The produced ingots of the alloys measured $\sim 6 \times 12 \times 40 \text{ mm}^3$. As-cast ingots were annealed at 1200 °C for 24 h. Prior to the annealing, the samples were encapsulated in vacuumed (10^{-2} Torr) quartz tubes filled with titanium chips to prevent any oxidation.

Microstructure and phase composition of the alloys after annealing at 1200 °C were studied using X-ray diffraction (XRD), scanning electron microscopy (SEM) and transmission electron microscopy (TEM). The XRD analysis was performed using RIGAKU diffractometer and CuK α radiation. The obtained XRD data were also used for calculation of a long-range order parameter (LROP) of the AlNbTiVZr_x alloys in accordance with the following equation:

$$LROP = (I_{sl}/I_{fund})(Lp_{fund}/Lp_{sl})(F_{fund}/F_{sl}), \quad (1)$$

where I_{sl} and I_{fund} are the intensities of the superlattice reflection and the fundamental reflection peaks from the alloy, respectively; Lp_{sl} and Lp_{fund} are parameters which include the Lorentz and the polarization factors and the geometry of the X-ray diffraction recording:

$$Lp_{fund} = (1 - \cos^2 2\theta_{fund}) / (\sin 2\theta_{fund} \sin \theta_{fund});$$

$$Lp_{sl} = (1 - \cos^2 2\theta_{sl}) / (\sin 2\theta_{sl} \sin \theta_{sl}), \quad (2)$$

where θ_{sl} and θ_{fund} are the Bragg angles for the fundamental and superlattice reflections, respectively; and F_{fund} and F_{sl} are the structure factors for the fundamental and superlattice lines, respectively. For the stoichiometric (50:50) composition of a B2 phase, the structure factors for the fundamental and superlattice lines are calculated as follows:

$$F_{fund} = f_{A,fund} + f_{B,fund}; F_{sl} = f_{A,sl} - f_{B,sl}, \quad (3)$$

where f_A and f_B are the atomic scattering factors for A and B elements, respectively. In the case of AlNbTiVZr_x alloys, it is impossible to define a stoichiometric composition of the B2 phase due to the simultaneous presence of a variety of constitutive elements. Therefore, based on a number of earlier studies [17–25] about the site occupations of alloying elements in ordered Ti alloys, the Ti sublattice (i.e. A sites) was assumed to be occupied with Ti, Nb and Zr, while Al and V enter into the Al sublattice (i.e. B sites). The final formula for the calculation of the LROP of the B2 phase in the AlNbTiVZr_x alloys can be written as:

$$LROP = (I_{sl}/I_{fund})(Lp_{fund}/Lp_{sl}) \left(\frac{f_{A,fund}^* + f_{B,fund}^*}{f_{A,sl}^* - f_{B,sl}^*} \right)^2, \quad (4)$$

Where $f_A^* = f_{Ti}(c_{Ti}/(c_{Ti} + c_{Nb})) + f_{Nb}(c_{Nb}/(c_{Ti} + c_{Nb})) + f_{Zr}(c_{Zr}/(c_{Ti} + c_{Zr}))$; $f_B^* = f_{Al}(c_{Al}/(c_{Al} + c_V)) + f_V(c_V/(c_{Al} + c_V))$; c_{Ti} , c_{Nb} , c_{Zr} , c_{Al} and c_V are the concentrations of the constitutive elements in the matrix phase, taken from Table 2.

Samples for SEM observations were prepared by mechanical polishing. SEM investigations were carried out using either FEI Quanta 600 FEG or Nova NanoSEM microscopes; both instruments were equipped with energy-dispersive (EDS) and electron backscattered diffraction (EBSD) detectors. The volume fraction of different phases was measured by a Digimizer Image Analysis Software using SEM-BSE images. Mechanically pre-thinned to 100 μm foils were prepared for TEM analysis by conventional twinjet electro-polishing at temperature of -35 °C and an applied voltage of 29.5 V in a mixture of 600 ml of methanol, 360 ml of butanol and 60 ml of perchloric acid. TEM investigations were performed using a JEOL JEM-2100 apparatus equipped with an EDS detector at an accelerating voltage of 200 kV.

The density of the annealed alloys was measured by hydrostatic weighting method. The density was measured on compressive specimens (see below), 3 samples of each alloy were measured.

Isothermal compression of rectangular specimens measured $6 \times 4 \times 4 \text{ mm}^3$ was carried out at 22 °C, 600 °C or 800 °C using an Instron

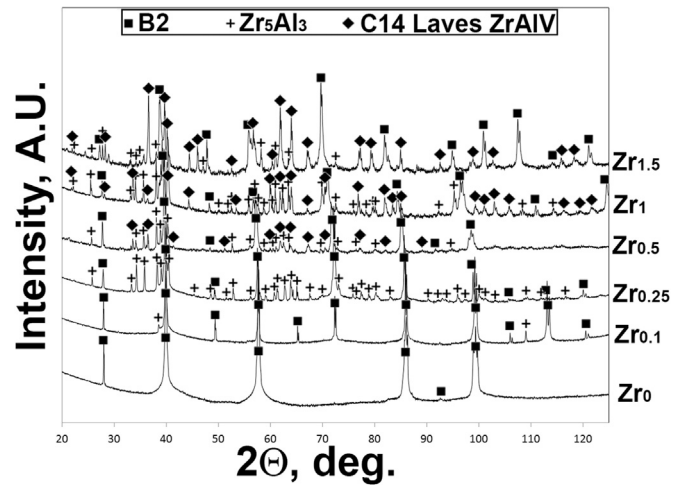


Fig. 1. XRD patterns of the AlNbTiVZr_x ($x = 0; 0.1; 0.25; 0.5; 1; 1.5$) alloys after annealing at 1200 °C for 24 h.

300LX test machine equipped with a radial furnace. The specimens were placed into the preheated to testing temperatures furnace and held for ≈ 10 min to equilibrate the temperature prior to testing. The temperature of the specimen was controlled by a thermocouple attached to a side surface of the specimen. The initial strain rate was 10^{-4} s^{-1} . Three samples of each alloy were tested at each temperature to obtain representative stress-strain curves.

3. Results

3.1. Structure of the AlNbTiVZr_x ($x = 0; 0.1; 0.25; 0.5; 1; 1.5$) alloys

Fig. 1 illustrates the XRD patterns of the AlNbTiVZr_x alloys after annealing at 1200 °C for 24 h. Table 1 summarizes data on some crystal lattice parameters of different phases. The microstructure of the AlNbTiV alloy composed of a single phase ordered B2 phase with the lattice parameters of $a_{B2} = 0.3186 \pm 0.0001 \text{ nm}$ (Fig. 1, Table 1). The AlNbTiVZr_{0.1} and AlNbTiVZr_{0.25} alloys consisted of the B2 and hexagonal Zr₅Al₃-type [26] phases (Fig. 1). The alloys with higher Zr content, namely the AlNbTiVZr_{0.5}, AlNbTiVZr and AlNbTiVZr_{1.5} alloys, were composed of the B2 phase, Zr₅Al₃-type phase and hexagonal C14 Laves phase of ZrAlV-type [27] (Fig. 1). The intensity of the Bragg peaks associated with the Laves phase of ZrAlV-type gradually increased with an increase in the Zr content (Fig. 1). The lattice parameter of the B2 phase demonstrated a gradual increase with an increasing in the Zr content (Table 1).

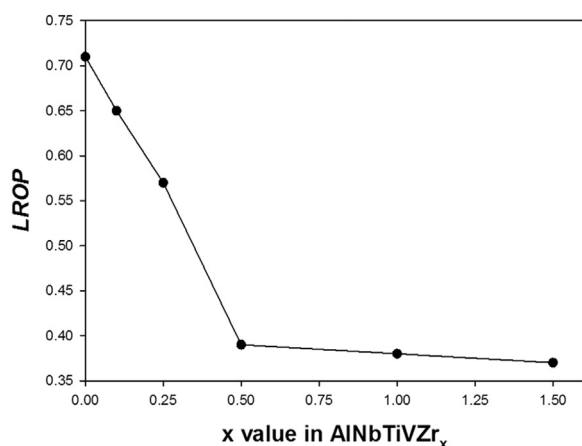
Values of the LROP as a function of the Zr content obtained for the matrix B2 phase of the AlNbTiVZr_x alloys are shown in Fig. 2. With an increase in the Zr percentage the LROP decreased pronouncedly from 0.71 for the Zr-free AlNbTiV alloy to 0.39 for the AlNbTiVZr_{0.5} alloy. Further increase in the Zr content resulted in rather weak reduction of the LROP to 0.38 and 0.37 for the AlNbTiVZr and AlNbTiVZr_{1.5} alloys, respectively.

Fig. 3 presents microstructures of the AlNbTiVZr_x ($x = 0; 0.1; 0.25; 0.5; 1; 1.5$) alloys after annealing at 1200 °C for 24 h; data on the chemical compositions, volume fractions and dimensions of the structural constituents are tabulated in Table 2. The AlNbTiV alloy had a single phase coarse-grained structure with the average size of $\sim 300 \mu\text{m}$ and the nominal chemical composition (Fig. 3a and Table 2). TEM investigation (Fig. 3b) has revealed the presence of thermal antiphase domains (APD). A selected area electron diffraction (SAED) pattern had shown the presence of (100) superlattice maxima which suggested the ordering of the B2 phase; this finding was consistent with the XRD data (Fig. 1).

The AlNbTiVZr_{0.1} alloy (Fig. 3c) had a coarse granular structure of

Table 1Lattice parameters of the constitutive phases of AlNbTiVZr_x (x = 0; 0.1; 0.25; 0.5; 1; 1.5) alloys after annealing at 1200 °C for 24 h.

Phase	Lattice parameter, nm		
	B2	Zr ₅ Al ₃ -type phase	C14 (hcp) Laves phase of ZrAlV-type
AlNbTiV	a = 0.3190 ± 0.0005	–	–
AlNbTiVZr _{0.1}	a = 0.3196 ± 0.0002	a = 0.8015 ± 0.0005, c = 0.5122 ± 0.0002	–
AlNbTiVZr _{0.25}	a = 0.3203 ± 0.0003	a = 0.7996 ± 0.0002, c = 0.5374 ± 0.0004	–
AlNbTiVZr _{0.5}	a = 0.3218 ± 0.0003	a = 0.8021 ± 0.0003, c = 0.5411 ± 0.0002	a = 0.5338 ± 0.0004, c = 0.8727 ± 0.0003
AlNbTiVZr	a = 0.3250 ± 0.0012	a = 0.8029 ± 0.0002, c = 0.5403 ± 0.0002	a = 0.5332 ± 0.0003, c = 0.8741 ± 0.0002
AlNbTiVZr _{1.5}	a = 0.3300 ± 0.0014	a = 0.7992 ± 0.0002, c = 0.5399 ± 0.0002	a = 0.5326 ± 0.0003, c = 0.8726 ± 0.0002

**Fig. 2.** The LROP as a function of Zr content.

mainly single phase; however a minor (< 1%) fraction of another phase (light-gray particles; marked as 2 in Fig. 3c) can also be observed. This secondary phase was found to be enriched with Zr and Al (Table 2). The same phase was also found in the AlNbTiVZr_{0.25} alloy (Fig. 3d) either in the form of a continuous network along the matrix grain boundaries or as individual particles inside grains. The volume fraction of this phase in the AlNbTiVZr_{0.25} alloy was ≈ 5% (Table 2).

The AlNbTiVZr_{0.5} alloy demonstrated a three-phase structure composed of a matrix phase (marked as 1 in Fig. 3e), light-gray particles enriched with Zr and Al (marked as 2 in Fig. 3e) and dark-gray particles, enriched with Zr, Al, and V (marked as 3 in Fig. 3e). The two last phases have been identified using TEM analysis as the Zr₅Al₃-type phase and C14 Laves phase of ZrAlV-type (the corresponding TEM micrograph and SAED pattern are not shown), respectively (Fig. 3f). TEM studies also revealed the presence of the APD and B2 ordering of matrix, like those in the AlNbTiV alloy (Fig. 3b). Both the Zr₅Al₃-type and ZrAlV-type phases were predominantly located along grain boundaries of the matrix phase as discontinuous chains of particles; however, some particles of the Zr₅Al₃-type phase were observed inside B2 grains. The volume fraction of the matrix phase, Zr₅Al₃-type phase, and ZrAlV-type Laves phase were found to be 85 ± 2, 5 ± 1 and 10 ± 2%, respectively. The average grain size of the matrix phase pronouncedly decreased with an increase in Zr content from 300 μm for the AlNbTiV alloy to 22 μm for the AlNbTiVZr_{0.5} alloy (Table 2).

The AlNbTiVZr and AlNbTiVZr_{1.5} alloys also had the three-phase structure and consisted of the ordered B2 matrix phase, Zr₅Al₃-type phase and ZrAlV-type Laves phase (Fig. 3g-i). The volume fraction of the Zr₅Al₃-type phase was 12 ± 2% for the AlNbTiVZr alloy and 5 ± 1% for the AlNbTiVZr_{1.5} alloy (Table 2). The volume fraction of the ZrAlV-type Laves phase increased to 21 ± 2% for the AlNbTiVZr alloy and to 45 ± 2% for the AlNbTiVZr_{1.5} alloy (Table 2). It should be noted that an increase in the Zr molar fraction resulted in a decrease in the Al content in the matrix phase from 27.4 at% for the AlNbTiV alloy to 13.7 at% for the AlNbTiVZr_{1.5} alloy (Table 2).

3.2. Density and mechanical properties of the AlNbTiVZr_x (x = 0; 0.1; 0.25; 0.5; 1; 1.5) alloys

The experimentally determined densities of the AlNbTiVZr_x alloys are given in Table 3. Zr resulted in a gradual increase in the density of the alloys from 5590 kg m⁻³ for the AlNbTiV alloy to 5870 kg m⁻³ for the AlNbTiVZr_{1.5} alloy. These values indicate the studied alloys belong to the light-weight refractory HEAs [6–8,12–16].

Fig. 4 displays engineering stress-strain curves of the AlNbTiVZr_x alloys obtained during compression at 22–800 °C; the resulting mechanical properties are summarized in Table 4 and Fig. 5. At 22 °C the yield strength of the alloys pronouncedly increased with an increase in Zr content. However, the increment of strength occurred non-monotonically; rapidly increased from 1000 MPa for the AlNbTiV alloy to 1485 MPa for the AlNbTiVZr_{0.5} alloy and then slightly rose to 1535 MPa for the AlNbTiVZr_{1.5} alloy. Besides, fast strengthening was observed in the AlNbTiVZr_x (x = 0; 0.1) alloys, whereas strengthening of the alloys with the higher Zr content occurred much slower. Plasticity of the AlNbTiVZr_x alloys showed a complicated dependence on the Zr content. The AlNbTiVZr_x (x = 0; 0.1; 0.25; 1; 1.5) alloys demonstrated low plasticity at room temperature; these alloys fractured at height reductions in a range from 0.4% for the AlNbTiVZr_{1.5} alloy to 9.3% for the AlNbTiVZr_{0.25} alloy (Figs. 4a and 5, Table 4). However, the AlNbTiVZr_{0.5} alloy exhibited high compression plasticity – over 50% (Figs. 4a and 5, Table 4). Several drops of flow stress at the stress-strain curve of the AlNbTiVZr_{0.5} alloy (Fig. 4a), which most likely were associated with cracking, are noteworthy. Careful macroscopic examination of the sample after the compression test revealed the presence of surface cracks. However, SEM microscopic analysis showed the formation of cracks within second phase particles only; these cracks did not propagate to the matrix. In turn, TEM investigation (Fig. 6) of the compressed sample has discovered that the structure of the matrix phase was a simple disordered bcc instead of the ordered B2 as in the initial state (Fig. 3f). The matrix phase of the alloy was chopped into rhomb-shaped areas by crossing deformation bands inclined by ~60° from the compression axis; in addition dense dislocation walls and pile-ups were observed in the microstructure.

An increase in testing temperature to 600 °C resulted in somewhat lower strength of the alloys (Figs. 4b and 5, Table 4). Similar to the room temperature behavior the yield strength of the alloys increased with the Zr content; the yield strength of the AlNbTiV and AlNbTiVZr_{1.5} alloys was found to be 780 and 1195 MPa, respectively. Strain hardening occurred in rather similar manner for all alloys with different Zr content. The increased temperature also results in plasticity enhancement of the AlNbTiV and AlNbTiVZr_{0.1} alloys. However, the alloys with the molar fraction of Zr ≥ 0.25 became less plastic. The most significant reduction in plasticity was observed for the AlNbTiVZr_{0.5} alloy, which fractured at 7.5% of strain. In general, plasticity of the AlNbTiVZr_x alloys at 600 °C decreased with an increase in Zr content from 14.3% for the AlNbTiV alloy to 0% for the AlNbTiVZr_{1.5} alloy.

At 800 °C, all the tested AlNbTiVZr_x alloys can be compressed up to 50% of height reduction without fracture (Figs. 4c and 5, Table 4). The dependence of the yield strength on the Zr content changed remarkably

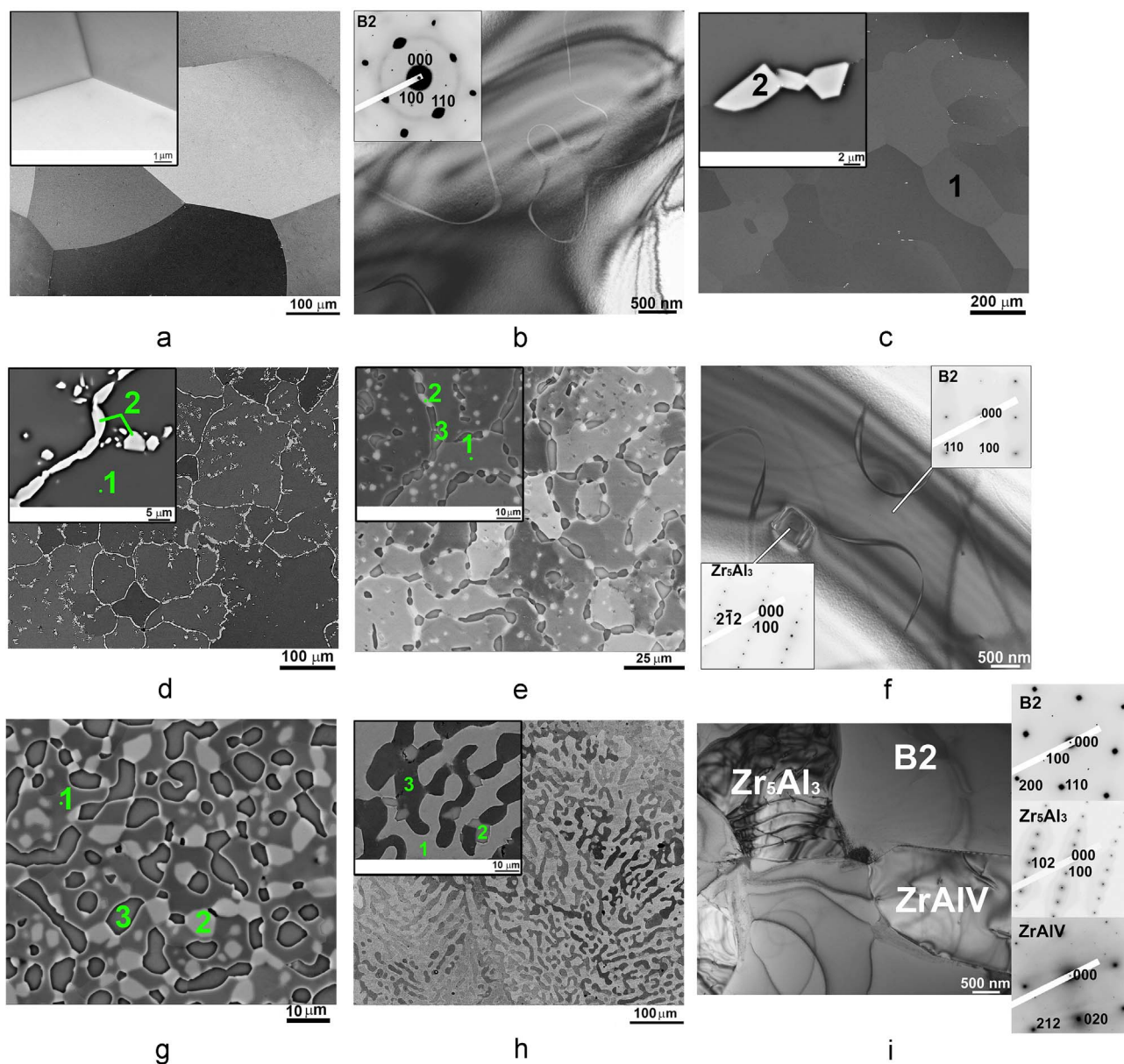


Fig. 3. Microstructure of the AlNbTiVZr_x alloys ($x = 0$ (a, b); 0.1 (c); 0.25 (d); 0.5 (e, f); 1 (g); 1.5 (h, i)) after annealing at 1200 °C for 24 h: a, c, d, e, g, h – SEM-BSE images, b, f, i – TEM bright-field images. Chemical compositions of the designated constituents are given in Table 2.

in comparison with the lower testing temperatures. The yield strength slightly increased from 560 MPa to 855–865 MPa with an increase in the molar fraction of Zr in the range of 0–0.1–0.25 and then monotonically decreases to 180 MPa with a further increment of the Zr content to the AlNbTiVZr_{1.5} alloy. Note that all the alloys exhibited softening during compression following the peak stress at the initial stages of deformation; the most pronounced softening was observed in the AlNbTiVZr_{0.1} and AlNbTiVZr_{0.25} alloys.

4. Discussion

4.1. Effect of Zr on the structure of the AlNbTiVZr_x alloys

The microstructure analysis of the AlNbTiVZr_x alloys with different Zr content, performed in the current study, has revealed several features. First, an increase in the Zr content substantially decreased the LROP of the matrix B2 phase of the alloys (Fig. 3). Second, an addition of Zr resulted in the formation of intermetallic phases, namely the Zr₅Al₃-type phase and the Laves phase of ZrAlV-type (Tables 1, 2). The

latter quite expected finding can be associated with a highly negative enthalpy of intermetallic phases formation in respective Zr-X binaries, where X are the other constituents (e.g. Al; for instance, the enthalpy of the binary Zr₅Al₃-type phase formation was $-51.5 \text{ kJ mol}^{-1}$ [28]). However, the B2 ordering of the matrix phase and the dependence of the LROP on the Zr content deserve more detailed discussion.

The B2 ordering is often observed in Al-containing high-entropy alloys [29–34]. Al was found to be a bcc/B2 stabilizer in those HEAs which are based on late transition metals (TMs) such as Fe, Ni, Co and Cu [29–35]. Having a high electron density (the outermost shell holds three electrons) and a high Fermi level (small work-function and high ionization tendency), Al prefers to transfer electrons to TMs, such as Ni, Co, Fe, Cr and Mn, to form intermetallic compounds with covalent bonds between the elements [36].

Meanwhile, the role of Al in HEAs based on refractory metals is not well-established so far. In a number of Al-containing refractory HEAs [11,12,15,37–39], the B2 ordering was not observed, and only a few studies [40,41] revealed the formation of the B2 phase in the presence of Al. Particularly, the B2 phase in the AlCrTiV alloy was shown to be

Table 2

Chemical compositions, volume fractions and dimensions of the structural constituents of the AlNbTiVZr_x (x = 0; 0.1; 0.25; 0.5; 1; 1.5) alloys after annealing at 1200 °C for 24 h. Analyzed areas are denoted in Fig. 3.

Elements, at.%		Al	Nb	Ti	V	Zr	Volume fraction, %	Average size, μm	
								transversal	longitudinal
Constituents		AlNbTiV							
№	Designation								
	Grains	27.4	24.2	24.6	23.8	–	100	300 ± 25	
Alloy composition		27.6	24.1	24.8	23.5	–	–	–	
		AlNbTiVZr _{0.1}							
1	Grains	25.4	23.4	24.8	23.2	3.2	> 99	175 ± 50	
2	Light-gray particles (Zr ₅ Al ₃ -type phase)	35.1	15.9	14.3	5.2	29.5	< 1	3.5 ± 0.6	
Alloy composition		25.7	23.6	24.6	22.8	3.3	–	–	
		AlNbTiVZr _{0.25}							
1	Grains	24.0	23.1	25.2	23.1	4.6	95 ± 2	80 ± 30	
2	Light-gray particles (Zr ₅ Al ₃ -type phase)	38.2	14.0	11.4	4.4	32.0	5 ± 1	2.5 ± 0.4	–
Alloy composition		25.0	22.4	24.0	21.9	6.7	–	–	
		AlNbTiVZr _{0.5}							
1	Matrix	21.0	23.0	24.8	22.9	8.3	85 ± 2	22 ± 12	
2	Light-gray particles (Zr ₅ Al ₃ -type phase)	38.2	13.1	10.7	4.6	33.4	5 ± 1	2.8 ± 1.0	
3	Dark-gray particles (ZrAlV-type Laves phase)	33.1	9.8	8.8	22.3	26.0	10 ± 2	3.7 ± 0.9	9.0 ± 2.5
Alloy composition		23.4	20.9	22.8	21.7	11.2	–	–	
		AlNbTiVZr							
1	Matrix	16.5	25.8	24.7	18.5	14.5	67 ± 3	–	
2	Light-gray particles (Zr ₅ Al ₃ -type phase)	38.7	9.5	8.3	3.6	39.9	12 ± 2	5.0 ± 0.5	
3	Dark-gray particles (ZrAlV-type Laves phase)	28.9	9.9	8.6	22.3	30.3	21 ± 2	5.3 ± 0.6	12.2 ± 5.0
Alloy composition		22.0	20.8	19.9	18.9	18.4	–	–	
		AlNbTiVZr _{1.5}							
1	Matrix	13.7	23.0	25.3	15.1	22.9	50 ± 2	–	
2	Light-gray particles (Zr ₅ Al ₃ -type phase)	33.7	12.2	9.9	3.8	40.4	5 ± 1	6.1 ± 1.9	
3	Dark-gray particles (ZrAlV-type Laves phase)	20.7	14.4	10.9	25.2	28.8	45 ± 2	8.0 ± 2.5	31.0 ± 6.5
Alloy composition		16.9	19.4	19.1	18.7	25.9	–	–	

Table 3

Density of the AlNbTiVZr_x (x = 0; 0.1; 0.25; 0.5; 1; 1.5) alloys.

Alloy	ρ, kg/m ³
AlNbTiV	5590
AlNbTiVZr _{0.1}	5530
AlNbTiVZr _{0.25}	5570
AlNbTiVZr _{0.5}	5640
AlNbTiVZr	5790
AlNbTiVZr _{1.5}	5870

more thermodynamically stable than the disordered bcc [41] whereas some other Al-containing refractory HEAs (e.g. Al_xNbTiMoV alloys [38]) were declared to be composed of single or several disordered bcc phases. This ambiguity can be partially ascribed to limitations of the techniques used for structural analysis. For instance, based on the XRD and SEM analysis the AlMo_{0.5}NbTa_{0.5}TiZr alloy [11] was found to be consisted of two disordered bcc phases. Further study by advanced TEM techniques has revealed the presence of an Al-Zr-rich B2 phase in this alloy [40]. In the case of the AlNbTiV alloy, the B2 ordering was not found previously [8,13] most likely due to lower quality of XRD data and the absence of TEM examinations. Thus, it can be suggested that more detailed (i.e. using TEM) investigation are needed to discover the B2 ordering in other Al-containing alloys. However, as it will be discussed further, the degree of ordering can be considerably dependent on the exact chemical composition of the alloy and therefore some Al-containing refractory HEAs can have disordered structures. Nevertheless, based on the already existed experimental data, the formation of the ordered B2 matrix phase in the studied AlNbTiVZr_x alloys can be attributed to the presence of Al.

Moreover, the LROP parameter of the B2 phase in the AlNbTiVZr_x alloys showed a pronounced dependence on the Zr content (Fig. 3). The dependence of the LROP of the ordered phase(s) on the chemical composition of HEAs has never been revealed so far. The Al-induced B2

ordering was earlier found in some β-Ti alloys [17–25]. It was demonstrated that both the bcc/B2 transformation and the degree of the order of the B2 phase in those alloys were depended on the Al content [17]. In the case of the AlNbTiVZr_x alloys, the Al concentration in the B2 phase decreased with an increase in the Zr content (Table 2). The decrease in Al concentration in the B2 phase can be associated with: (i) the proportional decrease in the concentration of other (than Zr) constitutive elements of the AlNbTiVZr_x alloys with the increase in X; (ii) preferred segregation of Al within the Zr-Al-rich intermetallic phases (Table 2). However, in the case of the AlNbTiVZr_x alloys, the LROP of the B2 phase was not in the direct proportion to the Al concentration. For example, the LROP decreased from 0.71 in the AlNbTiV alloy to 0.39 in the AlNbTiVZr_{0.5} alloy (Fig. 3) that corresponded to the decrease in the Al content in the B2 matrix from 27.4 at% to 21.0 at% (Table 2). However further decrease in the Al concentration in the B2 phase of the AlNbTiVZr_{1.5} alloy to 13.7 at% resulted only in a slight change in the LROP of the B2 phase, which was equal to 0.37. The absence of a linear relationship between the Al concentration and the LROP can be ascribed to the complexity in site occupancy in the B2 phase, similar to that in Ti alloys [42]. In Ti alloys the excessive Ti or Zr atoms (usually taking the A-sites, i.e. body-centered positions) can occupy the B-sites, corresponding to the ordered B2 component. However, to evaluate the site occupancy in the AlNbTiVZr_x alloys further in-depth study is needed.

Another interesting finding is the B2/bcc transition during the compression of the AlNbTiVZr_{0.5} alloy at 22 °C (Fig. 6). The order/disorder transition under deformation was often observed in binary intermetallic compounds with the B2 or L1₂ structures [43–48]. The disordering is a result of the movement of superlattice dislocations which contain antiphase boundaries (APB) [43–48]. In turn, the energy of APB was found to be depended on the LROP [48–50]. A decrease in the LROP lowers the APB energy thereby reducing the slip resistance and facilitating the glide of unit dislocations of superlattice dislocations [48–50]. It implies that the deformation-induced disordering will proceed easier and faster in structures with a low LROP rather than in those

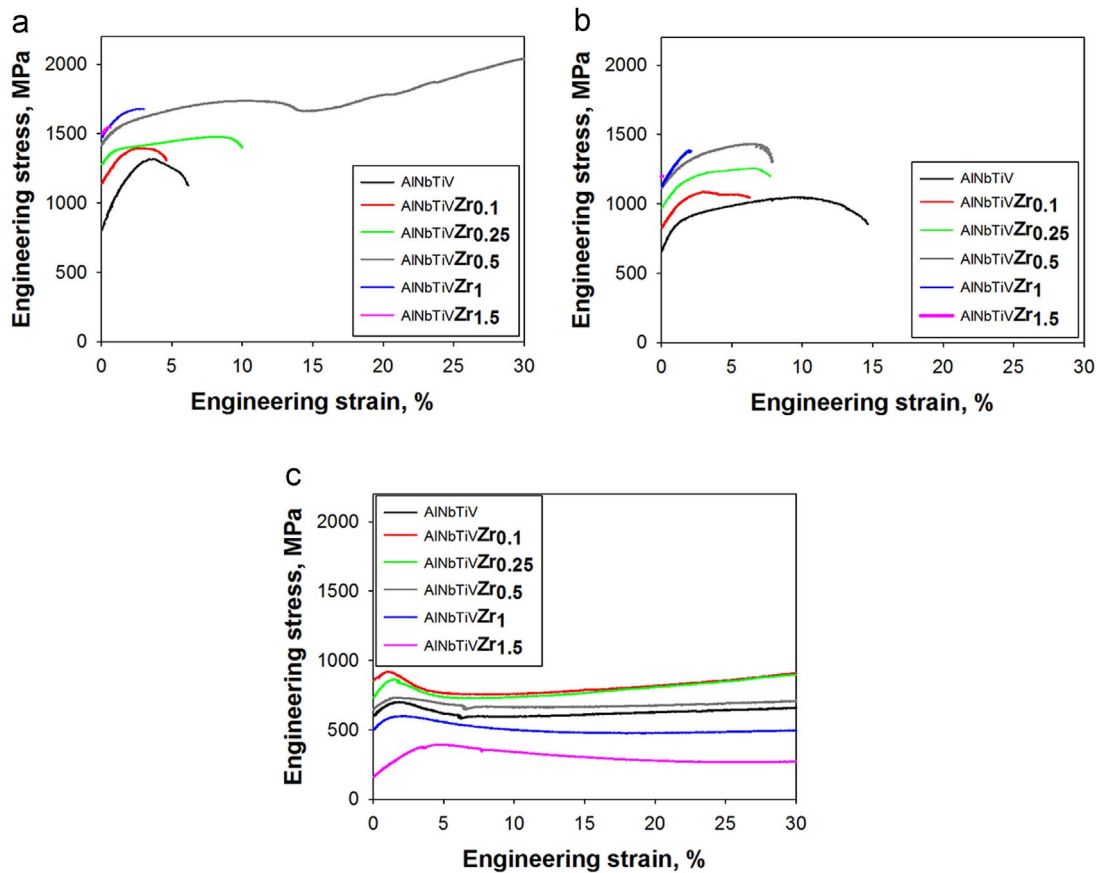


Fig. 4. Engineering stress-strain curves of the AlNbTiVZr_x (x = 0; 0.1; 0.25; 0.5; 1; 1.5) alloys obtained during compression at 22 °C (a), 600 °C (b) and 800 °C (c).

with a high LROP. Therefore, it can be suggested that the lower LROP of the B2 phase in the AlNbTiVZr_{0.5} alloy is responsible for the B2-bcc transition under plastic deformation at room temperature.

4.2. Effect of Zr on mechanical properties of the AlNbTiVZr_x alloys

The Zr content (X) has a prominent effect on the mechanical properties of the AlNbTiVZr_x alloys, as it can be expected from the pronounced changes in the microstructure. Both strength and plasticity of the studied alloys exhibited a complex dependence on the Zr content and temperature (Fig. 5).

According to previous data [12,13,15], two strengthening mechanisms were suggested to operate in the Al-Cr-Nb-Ti-V-Zr system alloys: (i) solid solution strengthening (SSS) and (ii) second phases strengthening. As Zr has the largest atomic radii (r_{Zr} = 160 p.m.) among the constituents of the AlNbTiVZr_x alloys, it may cause the strongest SSS due to the lattice distortions. Several attempts were made to evaluate the SSS in HEAs [51,52]. These calculations gave reasonable agreement with the strength of disordered HEAs; however theoretical

predictions are obviously inappropriate for ordered alloys like the AlNbTiVZr_x. To evaluate the SSS in the studied alloys a relationship between the increment in the yield strength of the AlNbTiVZr_x alloys Δσ (the difference between the yield strength of the Zr-containing alloys and the AlNbTiV alloy, Table 4), and the Zr concentration in the matrix B2 phase c_{Zr} (Table 2) [53] was plotted using the power law-type function:

$$\Delta\sigma \sim c_{Zr}^n \tag{5}$$

At n = 0.5 a good fit was obtained between Δσ and c_{Zr} for the AlNbTiVZr_x (x = 0; 0.1; 0.25; 0.5) alloys at T = 22 and 600 °C (Fig. 7). The value of n = 0.5 is typical for the classic Fleischer's approach for solid solution strengthening [54]. Therefore the strength increment in the AlNbTiVZr_x alloys with an increase in X from 0 to 0.5 at both 22 °C and 600 °C is thought to be the result of the SSS in the matrix. This finding is in a reasonable agreement with the relatively low fraction of the second phase particles, which approaches to 15% in the AlNbTiVZr_{0.5} alloy (Table 2). The morphology of the particles (large size, the preferred location at the grain boundaries) also suggests that they are

Table 4
The compression yield strength (σ_{YS}), peak stress (σ_p), and fracture strain (ε) of the AlNbTiVZr_x (x = 0; 0.1; 0.25; 0.5; 1; 1.5) alloys at 22–800 °C.

Temperature, °C	22			600			800		
	σ _{YS} , MPa	σ _p , MPa	ε, %	σ _{YS} , MPa	σ _p , MPa	ε, %	σ _{YS} , MPa	σ _p , MPa	ε, %
AlNbTiV	1000	1280	6.0	780	1005	14.3	560	700	> 50
AlNbTiVZr _{0.1}	1290	1395	3.7	975	1085	5.1	865	920	> 50
AlNbTiVZr _{0.25}	1360	1480	9.3	1065	1260	6.5	855	865	> 50
AlNbTiVZr _{0.5}	1485	–	> 50	1135	1425	7.5	675	740	> 50
AlNbTiVZr	1500	1675	3.0	1155	1385	1.0	550	600	> 50
AlNbTiVZr _{1.5}	1535	1550	0.4	1195	1195	0	180	395	> 50

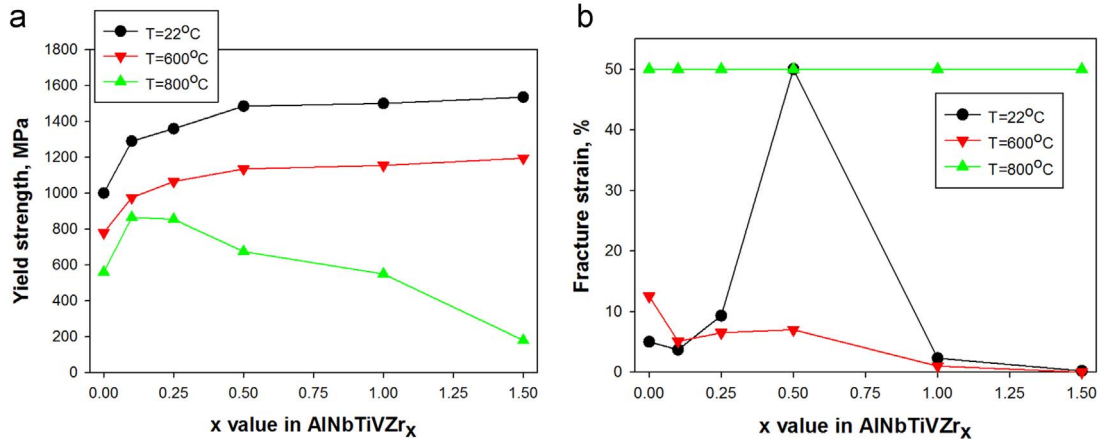


Fig. 5. The dependence of yield strength (a) and fracture strain (b) on the Zr content.

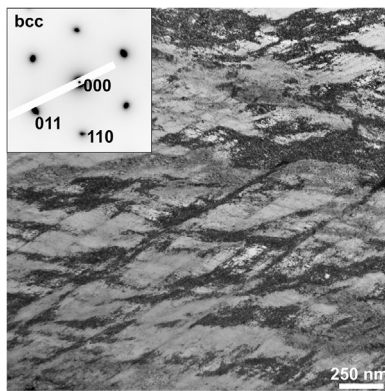


Fig. 6. TEM bright-field image of the AlNbTiVZr_{0.5} alloy after compression to 50% height reduction at 22 °C. The compression axis is vertical.

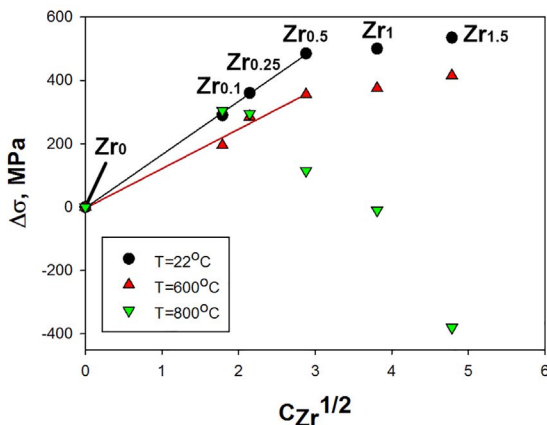


Fig. 7. The increment in the yield strength, $\Delta\sigma$, at T=22 and 600 °C as a function of the Zr concentration, c_{Zr} , in the matrix phase of the AlNbTiVZr_x alloys.

unlikely making a pronounced contribution to the strength of the alloys.

However, in the AlNbTiVZr_x (x = 0.5; 1; 1.5) alloys, the yield strength remains almost unchanged with an increase in X (Fig. 5a). This fact can be associated with a large volume fraction of the second phases in the alloys. Notably, the strengthening contribution of the second phase particles to the B2 ordered alloys was shown to be very small as the matrix phase is already very hard [55]. Moreover, in the present case, the second phase particles can even cause a negative effect on the strength. According to Eq. (5), the yield strength of the AlNbTiVZr_x alloys should increase steadily with an increase in X from 0 to 1.5 in

proportion with the Zr content in the B2 matrix (Table 2). But in the AlNbTiVZr_x (x = 0.5; 1; 1.5) alloys the increment of the strength of the matrix was compensated by some increase in the volume fraction of the presumably softer second phase particles (Table 2) and strength of the alloys stabilized.

At 800 °C the strength of the AlNbTiVZr_x alloys increased for X in the range of 0–0.25 reaching the maximum at X=0.1 (Fig. 5a). However for X within the interval of 0.25–1.5 the strength of the alloys, in contrast to the lower temperatures, decreased reaching the strength of the single phase AlNbTiV alloy at X = 1 and drastically dropping to the minimum at X = 1.5 (Fig. 5a). The effect of SSS is known to become weaker with an increase in temperature [51]. It can be clearly seen from Fig. 7 that the slope of the $\Delta\sigma - c_{Zr}$ line decreased with an increase in temperature from 22 °C to 600 °C. The SSS obviously became much weaker at 800 °C since no correlation between $\Delta\sigma$ and c_{Zr} for the whole Zr concentration range was found (Fig. 7). Thus some other factors controlling the yield strength of the AlNbTiVZr_x alloys should be considered.

In particular, one should keep in mind the ordered nature of the matrix phase and the changes in the LROP of the B2 phase. The strength of the ordered phases generally reduces with a lower rate with an increase in temperature in comparison with the strength of a disordered phase [56]. A high strength of the single phase AlNbTiV alloy at T=800 °C can be caused by the ordered B2 structure. Apparently, the strength of the B2 compounds depended on the LROP. This dependence is rather complicated; the maximum strength is often observed at some intermediate LROP values rather than at the maximum ones [50]. This finding is associated with an easier dissociation of the superlattice dislocations into unit dislocations acting as effective hardening sources at lower LROP values [50]. It can be supposed that in the present AlNbTiVZr_x alloys an increase in the yield strength at low Zr content (x = 0–0.25) was associated with two possible factors: (i) the SSS induced by Zr (which is weaker than at the lower temperatures, but still have some contribution) and (ii) changes in the LROP values of the matrix B2 phase (Fig. 2). However, in general, a decrease in the ordering degree beyond the certain value should decrease the high-temperature strength of the alloy [50]. Thus, a decrease in the LROP observed in the AlNbTiVZr_x alloys at X = 0.5, 1 or 1.5 (Fig. 2) possibly reduced the energy of the connecting APB considerably; as a result unit dislocations of superdislocations can be considered as ordinary dislocations which can glide independently and which do not produce considerable hardening at high temperatures [50]. Another reason for the lower strength of the AlNbTiVZr_x (x = 0.5; 1; 1.5) alloys can be associated with a large volume fraction of the second phases which possibly become much softer than the B2 ordered matrix at elevated temperatures.

The plasticity of the AlNbTiVZr_x alloys shows a complicated dependence on the Zr content, especially at room temperature (Fig. 5b).

The room temperature plasticity of the B2 alloys was dependent on the LROP; with a decrease in the ordering degree, the ductility increased [50]. A pronounced increase in the room temperature plasticity of the AlNbTiVZr_{0.5} alloy in comparison with the alloys with the lower Zr content can therefore be attributed to a pronounced decrease in the LROP (Fig. 2). Although further increase in the Zr content resulted in some decrease in the LROP (Fig. 2), the AlNbTiVZr and AlNbTiVZr_{1.5} alloys demonstrated a poor plasticity at room temperature (Fig. 5b). It is reasonable to believe that a high volume fraction of the second phases, and associated difficulties in strain compatibility between the particles of different phases, can result in a rapid failure during compression of the alloys.

At 600 °C, only the AlNbTiV alloy demonstrated a pronounced increment in the plasticity (Fig. 5b). The plasticity of the Zr-containing alloys remained almost unchanged, with an exception of the AlNbTiVZr_{0.5} alloy; its plasticity reduced almost by an order of magnitude. Nevertheless, the AlNbTiVZr_{0.5} alloy still had the highest plasticity among the Zr-containing alloys. The reasons for lowered plasticity at 600 °C remain unclear and need further in-depth study.

With the further increase in the temperature to T=800 °C, the AlNbTiVZr_x alloys demonstrated high compression plasticity (≥50%) regardless of the Zr content (Fig. 5b). This can be considered as an indication of the brittle-to-ductile transition occurring in the alloys in the interval of 600–800 °C. Most probably, the brittle-to-ductile transition is the consequence of an increase in dislocation mobility in the B2 ordered matrix with temperature increase.

In summary, the present study identified that the ordering (LROP) of high-entropy alloys based on refractory metals can be controlled by the modifying their chemical composition. Moreover, the degree of order has pronounced effect on mechanical properties of the alloys (both strength and plasticity are strongly affected). These findings open new pathways to tailor the properties of the high entropy alloys and thus offer additional opportunities for the alloy development for various advanced applications, including high-temperature structural materials.

5. Conclusions

In this study, structure and mechanical properties of the AlNbTiVZr_x (x = 0; 0.1; 0.25; 0.5; 1; 1.5) refractory high-entropy alloys after annealing at 1200 °C for 24 h were examined. Following conclusions were made:

- 1) The AlNbTiV alloy possessed the single phase ordered B2 structure. The AlNbTiVZr_x (x = 0.1; 0.25) alloys were composed of the B2 and hexagonal Zr₅Al₃-type phases. The phase composition of the AlNbTiVZr_x (x = 0.5; 1; 1.5) alloys was presented by the B2 phase, Zr₅Al₃-type phase and hexagonal C14 Laves phase of ZrAlV-type. The volume fraction of the second phases increased with an increase in the Zr content from < 1% for the AlNbTiVZr_{0.1} alloy to 50% for the AlNbTiVZr_{1.5} alloy.
- 2) The long-range order parameter (LROP) of the B2 phase was found to be depended on the Zr content. The LROP reduced with an increase in the Zr content from 0.71 for the AlNbTiV alloy to 0.37 for the AlNbTiVZr_{1.5} alloy.
- 3) Zr resulted in a gradual increase in the density of the alloys from 5590 kg m⁻³ for the AlNbTiV alloy to 5870 kg m⁻³ for the AlNbTiVZr_{1.5} alloy.
- 4) The strength of the AlNbTiVZr_x alloys changed significantly with an increase in the Zr content. The values of the yield strength at 22 °C raised rapidly from 1000 MPa for the AlNbTiV alloy to 1485 MPa for the AlNbTiVZr_{0.5} alloy, and from 780 MPa to 1135 MPa for the respective alloys at 600 °C. The strength increment at T=22 and 600 °C was associated with solid solution strengthening (SSS). Further increase in the Zr content did not result in a pronounced enhancement of strength: the yield strength of the AlNbTiVZr_{1.5}

alloy was 1535 MPa at 22 °C and 1195 MPa at 600 °C, respectively. At 800 °C, the maximum strength was demonstrated by the AlNbTiVZr_{0.1} alloy, whereas the AlNbTiVZr_{1.5} alloy was the softest. A decrease in strength of the AlNbTiVZr_x alloys at 800 °C with an increase in the Zr content was associated with a lowering of the LROP of the B2 phase and a large fraction of the soft second phase particles.

- 5) The plasticity of the AlNbTiVZr_x alloys had a complex dependence on the Zr content. At 22 °C, the plasticity increased from 6% for the AlNbTiV alloy to > 50% for the AlNbTiVZr_{0.5} alloy. The plasticity enhancement was associated with a reduction of the LROP of the B2 phase. The plasticity then dropped to 0.4% for the AlNbTiVZr_{1.5} alloy, supposedly due to the presence of a large volume fraction of the intermetallic second phases. At 600 °C, the plasticity of the AlNbTiV alloy increased up to 14.3%, while the Zr-containing alloys had lower plasticity. At 800 °C, all the AlNbTiVZr_x alloys were plastically deformed up to 50% of strain without fracture.
- 6) After compression test of the AlNbTiVZr_{0.5} alloy at 22 °C to 50% of height reduction, the initial B2 ordered matrix phase was found to be transformed into disordered bcc, i.e. plastic deformation of the alloy results in the B2-to-bcc transition.

Acknowledgment

The authors gratefully acknowledge the financial support from the Russian Science Foundation Grant no. 14-19-01104. The authors are grateful to the personnel of the Joint Research Center, "Technology and Materials", Belgorod State National Research University, for their assistance with the instrumental analysis.

References

- [1] J.W. Yeh, S.K. Chen, S.J. Lin, J.Y. Gan, T.S. Chin, T.T. Shun, C.H. Tsau, S.Y. Chang, Nanostructured high-entropy alloys with multiple principal elements: novel alloy design concepts and outcomes (+ 274), *Adv. Eng. Mater.* 6 (2004) 299–303, <http://dx.doi.org/10.1002/adem.200300567>.
- [2] Y. Zhang, T.T. Zuo, Z. Tang, M.C. Gao, K.A. Dahmen, P.K. Liaw, Z.P. Lu, Microstructures and properties of high-entropy alloys, *Prog. Mater. Sci.* 61 (2014) 1–93, <http://dx.doi.org/10.1016/j.pmatsci.2013.10.001>.
- [3] D.B. Miracle, O.N. Senkov, A critical review of high entropy alloys and related concepts, *Acta Mater.* 122 (2017) 448–511, <http://dx.doi.org/10.1016/j.actamat.2016.08.081>.
- [4] O.N. Senkov, G.B. Wilks, D.B. Miracle, C.P. Chuang, P.K. Liaw, Refractory high-entropy alloys, *Intermetallics* 18 (2010) 1758–1765, <http://dx.doi.org/10.1016/j.intermet.2010.05.014>.
- [5] O.N. Senkov, G.B. Wilks, J.M. Scott, D.B. Miracle, Mechanical properties of Nb₂₅Mo₂₅Ta₂₅W₂₅ and V₂₀Nb₂₀Mo₂₀Ta₂₀W₂₀ refractory high entropy alloys, *Intermetallics* 19 (2011) 698–706, <http://dx.doi.org/10.1016/j.intermet.2011.01.004>.
- [6] O.N. Senkov, S.V. Senkova, C. Woodward, D.B. Miracle, Low-density, refractory multi-principal element alloys of the Cr-Nb-Ti-V-Zr system: microstructure and phase analysis, *Acta Mater.* 61 (2013) 1545–1557, <http://dx.doi.org/10.1016/j.actamat.2012.11.032>.
- [7] O.N. Senkov, S.V. Senkova, D.B. Miracle, C. Woodward, Mechanical properties of low-density, refractory multi-principal element alloys of the Cr-Nb-Ti-V-Zr system, *Mater. Sci. Eng. A* 565 (2013) 51–62, <http://dx.doi.org/10.1016/j.msea.2012.12.018>.
- [8] N.D. Stepanov, D.G. Shaysultanov, G.A. Salishchev, M.A. Tikhonovsky, Structure and mechanical properties of a light-weight AlNbTiV high entropy alloy, *Mater. Lett.* 142 (2015) 153–155, <http://dx.doi.org/10.1016/j.matlet.2014.11.162>.
- [9] Rogal, F. Czerwinski, P.T. Jochym, L. Litynska-Dobrzynska, Microstructure and mechanical properties of the novel Hf₂₅Sc₂₅Ti₂₅Zr₂₅ equiatomic alloy with hexagonal solid solutions, *Mater. Des.* 92 (2016) 8–17, <http://dx.doi.org/10.1016/j.matdes.2015.11.104>.
- [10] B. Gludovatz, A. Hohenwarter, D. Catoor, E.H. Chang, E.P. George, R.O. Ritchie, A fracture-resistant high-entropy alloy for cryogenic applications, *Sci.* (80-.). 345 (2014) 1153–1158, <http://dx.doi.org/10.1126/science.1254581>.
- [11] O.N. Senkov, S.V. Senkova, C. Woodward, Effect of aluminum on the microstructure and properties of two refractory high-entropy alloys, *Acta Mater.* 68 (2014) 214–228, <http://dx.doi.org/10.1016/j.actamat.2014.01.029>.
- [12] N.D. Stepanov, N. Yu Yurchenko, D.G. Shaysultanov, G.A. Salishchev, M.A. Tikhonovsky, Effect of Al on structure and mechanical properties of Al_xNbTiVZr (x = 0, 0.5, 1, 1.5) high entropy alloys, *Mater. Sci. Technol. (U. Kingd.)* 31 (2015) 1184–1193, <http://dx.doi.org/10.1179/1743284715Y.0000000032>.
- [13] N.D. Stepanov, N.Y. Yurchenko, D.V. Skibin, M.A. Tikhonovsky, G.A. Salishchev,

- Structure and mechanical properties of the $\text{AlCr}_x\text{NbTiV}$ ($x = 0, 0.5, 1, 1.5$) high entropy alloys, *J. Alloy. Compd.* 652 (2015) 266–280, <http://dx.doi.org/10.1016/j.jallcom.2015.08.224>.
- [14] N.D. Stepanov, N.Y. Yurchenko, V.S. Sokolovsky, M.A. Tikhonovsky, G.A. Salishchev, An $\text{AlNbTiZr}_{0.5}$ high-entropy alloy combining high specific strength and good ductility, *Mater. Lett.* 161 (2015) 136–139, <http://dx.doi.org/10.1016/j.matlet.2015.08.099>.
- [15] N.Y. Yurchenko, N.D. Stepanov, D.G. Shaysultanov, M.A. Tikhonovsky, G.A. Salishchev, Effect of Al content on structure and mechanical properties of the $\text{Al}_x\text{CrNbTiVZr}$ ($x = 0; 0.25; 0.5; 1$) high-entropy alloys, *Mater. Charact.* 121 (2016) 125–134, <http://dx.doi.org/10.1016/j.matchar.2016.09.039>.
- [16] N.D. Stepanov, N.Y. Yurchenko, E.S. Panina, M.A. Tikhonovsky, S.V. Zherebtsov, Precipitation-strengthened refractory $\text{Al}_{0.5}\text{CrNbTi}_2\text{V}_{0.5}$ high entropy alloy, *Mater. Lett.* 188 (2016) 0–6, <http://dx.doi.org/10.1016/j.matlet.2016.11.030>.
- [17] Y.G. Li, P.A. Blenkinsop, M.H. Loretto, N.A. Walker, Effect of aluminium on deformation structure of highly stabilised beta-Ti-V-Cr alloys, *Mater. Sci. Technol.* 15 (1999) 151–155, <http://dx.doi.org/10.1179/mst.1998.14.8.732>.
- [18] M.H. Loretto, D. Hu, Y.G. Li, Microstructural studies on some ordered Ti-based alloys, *Intermetallics* 8 (2000) 1243–1249, [http://dx.doi.org/10.1016/S0966-9795\(00\)00035-2](http://dx.doi.org/10.1016/S0966-9795(00)00035-2).
- [19] M.H. Loretto, D. Horspool, R. Botten, D. Hu, Y.G. Li, D. Srivastava, R. Sharman, X. Wu, Controlling the properties of some ordered Ti-based alloys, *Mater. Sci. Eng. A*. 329–331 (2002) 1–6, [http://dx.doi.org/10.1016/S0921-5093\(01\)01492-7](http://dx.doi.org/10.1016/S0921-5093(01)01492-7).
- [20] A.K. Singh, S. Banumathy, D. Sowjanya, M.H. Rao, On the structure of the B2 phase in Ti-Al-Mo alloys, *J. Appl. Phys.* 103 (2008), <http://dx.doi.org/10.1063/1.2931004>.
- [21] R. Kainuma, I. Ohnuma, K. Ishikawa, K. Ishida, Stability of B2 ordered phase in the Ti-rich portion of Ti-Al-Cr and Ti-Al-Fe ternary systems, *Intermetallics* 8 (2000) 869–875, [http://dx.doi.org/10.1016/S0966-9795\(00\)00016-9](http://dx.doi.org/10.1016/S0966-9795(00)00016-9).
- [22] K. Das, S. Das, Order-disorder transformation of the body centered cubic phase in the Ti-Ai-X ($X = \text{Ta, Nb, or Mo}$) system, *J. Mater. Sci.* 38 (2003) 3995–4002, <http://dx.doi.org/10.1023/A:1026262616194>.
- [23] M. Premkumar, A.K. Singh, Deformation behavior of an ordered B2 phase in Ti-25Al-25Zr alloy, *Intermetallics* 18 (2010) 199–201, <http://dx.doi.org/10.1016/j.intermet.2009.07.015>.
- [24] K.J. Leonard, V.K. Vasudevan, Site occupancy preferences in the B2 ordered phase in Nb-rich Nb-Ti-Al alloys, *Mater. Sci. Eng. A*. 329–331 (2002) 461–467, [http://dx.doi.org/10.1016/S0921-5093\(01\)01621-5](http://dx.doi.org/10.1016/S0921-5093(01)01621-5).
- [25] N. Kazantseva, V. Sazonova, G. Lyzhina, Effect of the annealing temperature on the long-range order in the B2 phase of the Ti-Al-Nb (Zr, Mo) alloy, *Phys. Met.* 102 (2006) 288–294, <http://dx.doi.org/10.1134/S0031918X06090080>.
- [26] Zr_5Al_3 . http://crystdb.nims.go.jp/crystdb/search-details?Substance_id=6003&tabDetail=pageD&need_more_value=&pageD=1&reference_id=4294995636&pageA=1&pageSubP=0&errorCode=0&pageSubD=1&pageSubA=1&isVisiblePeriodicTable=false&tab=pageA&tabSub=pageA&isNeedMoreValueError=false&search-type=search-materials&condition_type=chemical_system&pageS=1&pageP=0&pageSubS=1&condition_value=Zr+Al&need_more_type=prototype_number&material_id=4295346562&page=1&isConditionValueError=false.
- [27] ZrAlV . http://crystdb.nims.go.jp/crystdb/search-details?Substance_id=30593&tabDetail=pageD&need_more_value=&pageD=1&reference_id=4295036730&pageA=1&pageSubP=0&errorCode=0&pageSubD=1&pageSubA=1&isVisiblePeriodicTable=false&tab=pageA&tabSub=pageA&isNeedMoreValueError=false&search-type=search-materials&condition_type=chemical_system&pageS=1&pageP=0&pageSubS=1&condition_value=Zr+Al+V&need_more_type=prototype_number&material_id=4295503466&page=1&isConditionValueError=false.
- [28] T. Wang, Z. Jin, J.-C. Zhao, Thermodynamic assessment of the Al-Zr binary system, *J. Phase Equilibria*. 22 (2001) 544–551, <http://dx.doi.org/10.1361/105497101770332695>.
- [29] C.-J. Tong, Y.-L. Chen, J.-W. Yeh, S.-J. Lin, S.-K. Chen, T.-T. Shun, C.-H. Tsau, S.-Y. Chang, Microstructure characterization of $\text{Al}_x\text{CoCrCuFeNi}$ high-entropy alloy system with multiprincipal elements, *Metall. Mater. Trans. A*. 36 (2005) 881–893, <http://dx.doi.org/10.1007/s11661-005-0283-0>.
- [30] Y.F. Kao, T.J. Chen, S.K. Chen, J.W. Yeh, Microstructure and mechanical property of as-cast, -homogenized, and -deformed $\text{Al}_x\text{CoCrFeNi}$ ($0 \leq x \leq 2$) high-entropy alloys, *J. Alloy. Compd.* 488 (2009) 57–64, <http://dx.doi.org/10.1016/j.jallcom.2009.08.090>.
- [31] C. Li, J.C. Li, M. Zhao, Q. Jiang, Effect of aluminum contents on microstructure and properties of $\text{Al}_x\text{CoCrFeNi}$ alloys, *J. Alloy. Compd.* 504 (2010) S515–S518, <http://dx.doi.org/10.1016/j.jallcom.2010.03.111>.
- [32] W.R. Wang, W.L. Wang, J.W. Yeh, Phases, microstructure and mechanical properties of $\text{Al}_x\text{CoCrFeNi}$ high-entropy alloys at elevated temperatures, *J. Alloy. Compd.* 589 (2014) 143–152, <http://dx.doi.org/10.1016/j.jallcom.2013.11.084>.
- [33] Y. Ma, B. Jiang, C. Li, Q. Wang, C. Dong, P. Liaw, F. Xu, L. Sun, The BCC/B2 Morphologies in $\text{Al}_x\text{NiCoFeCr}$ high-entropy alloys, *Met. (Basel)* 7 (2017) 57, <http://dx.doi.org/10.3390/met7020057>.
- [34] D.G. Shaysultanov, G.A. Salishchev, Y.V. Ivanisenko, S.V. Zherebtsov, M.A. Tikhonovsky, N.D. Stepanov, Novel $\text{Fe}_{36}\text{Mn}_{21}\text{Cr}_{18}\text{Ni}_{15}\text{Al}_{10}$ high entropy alloy with bcc/B2 dual-phase structure, *J. Alloy. Compd.* (2017), <http://dx.doi.org/10.1016/j.jallcom.2017.02.211>.
- [35] T. Yang, S. Xia, S. Liu, C. Wang, S. Liu, Y. Zhang, J. Xue, S. Yan, Y. Wang, Effects of Al addition on microstructure and mechanical properties of $\text{Al}_x\text{CoCrFeNi}$ High-entropy alloy, *Mater. Sci. Eng. A*. 648 (2015) 15–22, <http://dx.doi.org/10.1016/j.msea.2015.09.034>.
- [36] Z. Tang, M.C. Gao, H. Diao, T. Yang, J. Liu, T. Zuo, Y. Zhang, Z. Lu, Y. Cheng, Y. Zhang, K.A. Dahmen, P.K. Liaw, T. Egami, Aluminum alloying effects on lattice types, microstructures, and mechanical behavior of high-entropy alloys systems, *Jom* 65 (2013) 1848–1858, <http://dx.doi.org/10.1007/s11837-013-0776-z>.
- [37] O.N. Senkov, C. Woodward, D.B. Miracle, Microstructure and properties of aluminum-containing refractory high-entropy alloys, *Jom* 66 (2014) 2030–2042, <http://dx.doi.org/10.1007/s11837-014-1066-0>.
- [38] S.Y. Chen, X. Yang, K.A. Dahmen, P.K. Liaw, Y. Zhang, Microstructures and crackling noise of $\text{Al}_x\text{NbTiMoV}$ high entropy alloys, *Entropy* 16 (2014) 870–884, <http://dx.doi.org/10.3390/e16020870>.
- [39] C.M. Lin, C.C. Juan, C.H. Chang, C.W. Tsai, J.W. Yeh, Effect of Al addition on mechanical properties and microstructure of refractory $\text{Al}_x\text{HfNbTaTiZr}$ alloys, *J. Alloy. Compd.* 624 (2015) 100–107, <http://dx.doi.org/10.1016/j.jallcom.2014.11.064>.
- [40] J.K. Jensen, B.A. Welk, R.E.A. Williams, J.M. Sosa, D.E. Huber, O.N. Senkov, G.B. Viswanathan, H.L. Fraser, Characterization of the microstructure of the compositionally complex alloy $\text{Al}_1\text{Mo}_{0.5}\text{Nb}_1\text{Ta}_{0.5}\text{Ti}_1\text{Zr}_1$, *Scr. Mater.* 121 (2016) 1–4, <http://dx.doi.org/10.1016/j.scriptamat.2016.04.017>.
- [41] Y. Qiu, Y.J. Hu, A. Taylor, M.J. Styles, R.K.W. Marceau, A.V. Ceguerra, M.A. Gibson, Z.K. Liu, H.L. Fraser, N. Birbilis, A lightweight single-phase AlTiVCr compositionally complex alloy, *Acta Mater.* 123 (2017) 115–124, <http://dx.doi.org/10.1016/j.actamat.2016.10.037>.
- [42] M. Premkumar, K.S. Prasad, A.K. Singh, Structure and stability of the B2 phase in Ti-25Al-25Zr alloy, *Intermetallics* 17 (2009) 142–145, <http://dx.doi.org/10.1016/j.intermet.2008.10.009>.
- [43] T. Material, E. Technique, Solid-state Physics Order – Disorder Phase Transition Induced By Plastic Strain in Cu_3Pd , 43 (2000) 615–620.
- [44] D.G. Morris, X. Amils, S. Surinach, M.D. Baro, M.A. Munoz-Morris, Disordering of B2 intermetallics by ball milling, with particular attention to FeAl, *Int. J. Non-Equilibrium Process.* 11 (2000) 379–409, <http://dx.doi.org/10.4028/www.scientific.net/MSF.360-362.195>.
- [45] C. Rentenberger, H.P. Karnthaler, On the evolution of a deformation induced nanostructure in a Ni_3Al alloy, *Acta Mater.* 53 (2005) 3031–3040, <http://dx.doi.org/10.1016/j.actamat.2005.03.016>.
- [46] C. Rentenberger, H.P. Karnthaler, Extensive disordering in long-range-ordered Cu_3Au induced by severe plastic deformation studied by transmission electron microscopy, *Acta Mater.* 56 (2008) 2526–2530, <http://dx.doi.org/10.1016/j.actamat.2008.01.035>.
- [47] D. Geist, C. Gammer, C. Mangler, C. Rentenberger, H.P. Karnthaler, Electron microscopy of severely deformed Li_2 intermetallics, *Philos. Mag.* 90 (2010) 4635–4645, <http://dx.doi.org/10.1080/14786435.2010.482178/r10>.
- [48] H. Li, Y.F. Liang, W. Yang, F. Ye, J.P. Lin, J.X. Xie, Disorder induced work softening of Fe-6.5wt%Si alloy during warm deformation, *Mater. Sci. Eng. A*. 628 (2015) 262–268, <http://dx.doi.org/10.1016/j.msea.2015.01.058>.
- [49] K. Raviprasad, K. Aoki, K. Chattopadhyay, The nature of dislocations and effect of order in rapidly solidified Fe(5.5-7.5)wt%Si alloys, *Mater. Sci. Eng. A*. 172 (1993) 125–135, [http://dx.doi.org/10.1016/0921-5093\(93\)90432-E](http://dx.doi.org/10.1016/0921-5093(93)90432-E).
- [50] N.S. Stoloff, R.G. Davies, The plastic deformation of ordered FeCo and Fe_3Al alloys, *Acta Mater.* 12 (1964) 473–485, [http://dx.doi.org/10.1016/0001-6160\(64\)90019-7](http://dx.doi.org/10.1016/0001-6160(64)90019-7).
- [51] I. Toda-Caraballo, P.E.J. Rivera-Díaz-Del-Castillo, Modelling solid solution hardening in high entropy alloys, *Acta Mater.* 85 (2015) 14–23, <http://dx.doi.org/10.1016/j.actamat.2014.11.014>.
- [52] N.D. Stepanov, D.G. Shaysultanov, M.A. Tikhonovsky, G.A. Salishchev, Tensile properties of the Cr-Fe-Ni-Mn non-equiatomic multicomponent alloys with different Cr contents, *Mater. Des.* 87 (2015) 60–65, <http://dx.doi.org/10.1016/j.matdes.2015.08.007>.
- [53] J. Rösler, H. Harders, M. Bäker, Mechanical Behaviour of Engineering Materials (2006). doi:10.3386/w1416.
- [54] R.L. Fleischer, Substitutional solution hardening, *Acta Metall.* 11 (1963) 203–209, [http://dx.doi.org/10.1016/0001-6160\(63\)90213-X](http://dx.doi.org/10.1016/0001-6160(63)90213-X).
- [55] J.D. Cotton, The effects of chromium on NiAl intermetallic alloys: part 1, *Microstruct. Mech. Prop.* 1 (1993) 3–20.
- [56] R.L. Fleischer, Intermetallic Compounds for Strong High-Temperature Materials (1989).